RSC Advances

ROYAL SOCIETY OF CHEMISTRY

www.rsc.org/advances

A Table of Contents Entry

A one-pot synthesis strategy was developed to prepare magnetic molecularly imprinted microspheres for selective recognition and fast removal of 17-beta-estrodiol.

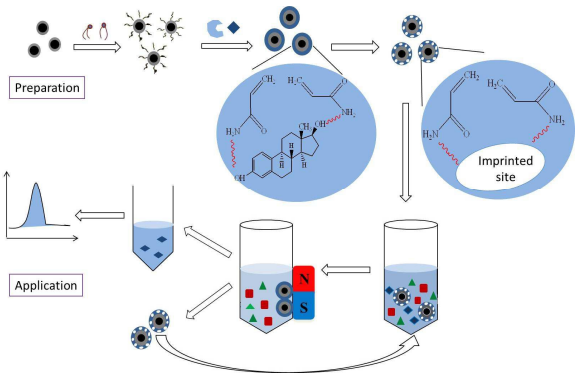

Cite this: DOI: 10.1039/c0xx00000x

www.rsc.org/xxxxxx

ARTICLE TYPE

One-pot synthesis of magnetic molecularly imprinted microspheres by RAFT precipitation polymerization for fast and selective removal of 17β-estradiol

Jinhua Li,[1a] Ruichen Dong,[1ab] Xiaoyan Wang,[c] Hua Xiong,*[b] Shoufang Xu,[ad] Dazhong Shen,*[c] Xingliang Song[d] and Lingxin Chen*[a]

Received (in XXX, XXX) Xth XXXXXXXXX 20XX, Accepted Xth XXXXXXXXX 20XX
DOI: 10.1039/b000000x

A facile strategy was developed to prepare magnetic molecularly imprinted microspheres (MMIMs) for selective recognition and effective removal of 17-beta-estradiol (17β-E2) by reversible addition-fragmentation chain transfer precipitation polymerization. One-pot synthesis was employed, which could simplify the imprinting process and shorten the experimental period. The resultant MMIMs displayed fast kinetics and high binding capacity, and the adsorption processes followed Langmuir-Freundlich isotherm and pseudo-second-order kinetic models. Excellent recognition selectivity toward 17β-E2 was attained over other phenolic estrogens such as 17-alpha-E2, estriol and estrone. The magnetic property of MMIMs provided fast and simple separation, and the recycling process for magnetic solid phase extraction (MSPE) was sustainable at least five times without obvious efficiency decrease. Furthermore, the MMIMs-MSPE presented satisfactory recoveries within 71.7–108.3% with the precisions of 1.1–6.0% for spiked 17β-E2 in water, soil and food samples. The developed MMIMs-based method proved to be a convenient and practical way in sample pretreatment and targeted pollutants removal.

1. Introduction

Estrogens, one class of important endocrine disrupting chemicals (EDCs), have become wide concerns due to their widespread presence and possible adverse impacts on the endocrine systems in wildlife and humans. Among estrogens, the most potent 17-beta-estradiol (17β-E2), a type of phenolic estrogens (PEEs), can damage the endocrine systems and even cause cancer and death at low-ng/L concentrations.[1,2] Moreover, it is difficult to separate by conventional treatment methods in complex matrices, resulting in the formation of by-products with even higher endocrine disrupting actions.[3,4] Thus, recognition, determination and elimination of 17β-E2 in complicated matrices at low concentrations have great practical significance and attract increasing studies, but still face severe challenges especially for selective separation, enrichment and removal.[5]

Recently, a number of reports using versatile, robust and cost-effective molecularly imprinted polymers (MIPs)[6] to specifically recognize, detect and remove 17β-E2 from polluted water and foods have been demonstrated. For examples, Ma *et al.* prepared selective core-shell MIPs of 17β-E2 on the surface of silica nanoparticles.[7] Shi *et al.* introduced molecularly imprinted solid phase extraction (MISPE) combined with HPLC to detect trace 17β-E2 in different dairy and meat samples.[8] Noir *et al.* fabricated macroporous MIP/cryogel composite systems for removing trace endocrine disrupting contaminants.[9] Usually, MIPs are synthesized by traditional free radical polymerization, whereas the rate of chain propagation cannot be controlled, resulting in a broad size distribution. The introduction of reversible addition-fragmentation chain transfer (RAFT) polymerization techniques into molecular imprinting strategy has attracted significant interest, which can solve the above problem.[10–14] For examples, Pan *et al.* described an approach to obtain water-compatible MIPs by the facile surface-grafting of functional polymer brushes *via* RAFT polymerization.[10] Titirici *et al.* prepared thin film MIPs around mesoporous silica beads by adopting covalent immobilization of azo initiators and RAFT-mediated living radical polymerization.[11] Our group presented atrazine MIPs for preconcentration of atrazine in food matrices by using di-thioesters based RAFT coupled to precipitation polymerization.[12,13]

Meanwhile, magnetic MIPs have received wide attentions since they can be easily isolated/collected and recycled by an external magnetic field and have been applied in many fields such as separation/purification, chemo/biosensing, drug delivery, and so on.[15–19] For instances, Li *et al.* synthesized a core-shell magnetic imprinted polymer for the fast and selective removal of EDCs.[18] Our group successfully prepared photonic/magnetic dual-responsive MIPs for recognition of caffeine.[19]

Herein, inspired by these studies, we developed an improved core-shell MIPs synthesis strategy for enhanced selective recognition and removal of 17β-E2 by combining RAFT

precipitation polymerization and magnetic separation. One-pot synthesis was conducted, allowing all reagents to react together under proper conditions. And the resultant MIPs layer was grafted onto the surface of magnetic iron oxide beads by RAFT agent for improving the polymerization efficiency. The obtained magnetic molecularly imprinted microspheres (MMIMs) were well characterized by morphologies, structures, thermostability and magnetism, as well as static and dynamic adsorptions. Finally, the MMIMs were used as SPE sorbents and successfully applied to the extraction of 17β-E2, providing a practicable way in samples pretreatment and removal of trace targeted pollutants in environment and food.

2. Experimental

2.1. Materials and apparatus

$FeCl_3·6H_2O$, carbon disulfide (CS_2), tetraethoxysilane (TEOS) and ammonia were purchased from Tianjin Chemical Reagents Company (Tianjin, China). 17-beta-estradiol (17β-E2) and acetonitrile were purchased from J&K Technology Limited (Beijing, China). 17-alpha-estradiol (17α-E2) and estriol (E3) were obtained from Dr. Ehrenstorfer (Germany). Estrone (E1), diethylstilbestrol (DES), hexestrol (HS), dienestrol (DS), and divinylbenzene (DVB) were provided by Sigma-Aldrich (Shanghai, China). Bisphenol A (BPA) and phenyl magnesium bromide (PMB) were supplied by Aladdin (Shanghai, China). Tetrahydrofuran (THF), acrylamide (AA), glycol and triethylamine were purchased from Kermel (Tianjin, China). 4-(chlormethyl)-phenyltrichlorosilane (4-CPS) was purchased from Alfa Aesar (Tianjin, China). All other reagents such as 2,2'-azobisisobutyronitrile (AIBN), trichloromethane, toluene and acetone were supplied by Sinopharm Chemical Reagent Co. Ltd. (Shanghai, China). Prior to use, THF was refluxed over sodium and then distilled; toluene and DVB were distilled in vacuum, and AIBN and AA were recrystallized in methanol and water, respectively. Deionized water used throughout the work was produced by a Milli-Q Ultrapure water system with the water outlet operating at 18.2 MΩ (Millipore, Bedford, USA).

The morphological evaluation was performed by transmission electron microscope (TEM, JEOL-100CX-2). Infrared spectra were recorded using Fourier transform infrared spectrometer (FT/IR-4100, Thermo Nicolet Corporation, USA). Thermal gravimetric analysis (TGA) was carried out from room temperature to 800 °C with a heating rate of 10 °C/min under nitrogen environment by thermal gravimetric analyzer (Mettler 5 MP), presenting TGA and derivative thermogravimetry (DTG) data. Magnetic property was measured by vibrating sample magnetometer (VSM, Lake Shore 7410, Beijing, China). UV-Vis spectra were recorded using a Thermo Scientific NanoDrop 2000/2000c spectrophotometer (Thermo, USA). N_2 adsorption-desorption isotherms were examined with Beishide instruments (3H-2000PS4, Beijing) for Brunauer, Emmett and Teller (BET) analysis to determine the specific surface area and pore size. The amounts of analytes were determined by HPLC-UV (Skyray LC-310, Skyray Instrument Inc., China), under the optimized conditions: sample loaded, 20 μL; mobile phase, acetonitrile/water (v/v, 7:3); flow rate, 1.0 mL/min; detection wavelength, 208 nm; column, 250 mm × 4.6 mm C_{18} at 20 °C.

2.2. Synthesis of Fe_3O_4@SiO_2 microspheres

Magnetic Fe_3O_4@SiO_2 microspheres were synthesized according to that reported[18] with slight modification. Fe_3O_4 nanoparticles were firstly prepared by solvothermal reduction method. Typically, 1.35 g $FeCl_3·6H_2O$ was dissolved in 40 mL glycol in a 100 mL flask with vigorously stirring. Then 2.0 g CH_3COONa and 3.0 g polyethylene glycol were added into the solution. After ultrasonic treatment for 30 min, the solutions were transferred to a 50 mL Teflon-lined autoclave and reacted for 10 h in a 200 °C oven, and the black Fe_3O_4 resultants were collected. Subsequently, 100 mg Fe_3O_4 nanoparticles were dispersed into 100 mL ethanol-water solvent (v/v, 3:1) in a 250 mL round flask and ultrasonic treatment for 10 min. Then 5 mL $NH_3·H_2O$ and 2 mL TEOS were added dropwise. After reaction for 12 h with constantly stirring at room temperature, the brown black resultants Fe_3O_4@SiO_2 was washed with plenty of ethanol and water, and dried under vacuum at 50 °C.

2.3. Synthesis of Fe_3O_4@SiO_2-RAFT microspheres

Magnetic Fe_3O_4@SiO_2-RAFT microspheres were synthesized according to the reported procedure[20] with necessary modification. Briefly, 1.0 g Fe_3O_4@SiO_2 microspheres were dispersed in 50 mL anhydrous toluene in a 100 mL three-necked flask by sonication for 15 min, followed by the addition of 2 mL 4-CPS and 1 mL triethylamine dropwise. After heated at reflux for 24 h under nitrogen protection, the modified Fe_3O_4@SiO_2 particles were washed, dried and collected. 3.0 mL CS_2 was added into 100 mL THF solution containing 10 mL PMB, and reacted for 2 h at 45 °C. Subsequently, 0.5 g modified Fe_3O_4@SiO_2 particles were dispersed in the mixed solution and stirred for 48 h at 65 °C under N_2 atmospheres, and the resultant products were washed with acetone and toluene repeatedly and dried under vacuum at 60 °C for 24 h. The brown resultants were marked as Fe_3O_4@SiO_2-RAFT.

2.4. Preparation of magnetic core-shell polymer microspheres

Core-shell imprinted polymer microspheres for 17β-E2 were prepared by one-pot RAFT precipitation polymerization. Typically, 0.1 mmol 17β-E2 and 0.6 mmol AA were dispersed in 10 mL toluene and 40 mL acetonitrile solution, and then 100 mg Fe_3O_4@SiO_2-RAFT, 2 mmol DVB and 20 mg AIBN were added in sequence. The resultant mixture was stirred at 70 °C for 24 h under N_2 protection. The product was washed with acetone for several times and then eluted by Soxhlet extraction with methanol/acetic solvent (9:1, v/v) for 24 h until no template detected. The obtained gray particles, *i.e.* magnetic molecularly imprinted microspheres (MMIMs), were dried to constant weight under vacuum at 40 °C, for use. The preparation process was schematically depicted in Fig. 1. On the other hand, magnetic non-imprinted microspheres (MNIMs) were also prepared by the same protocol without the addition of template. Besides, as control, Fe_3O_4@SiO_2 microspheres were added for one-pot precipitation polymerization reaction directly without adding RAFT agent, and the resultant dark gray particles were named as MMIMs-Control.

2.5. Binding property studies of the magnetic microspheres

Cite this: DOI: 10.1039/c0xx00000x

www.rsc.org/xxxxxx

ARTICLE TYPE

Binding properties of the prepared MMIMs, MNIMs and MMIMs-Control were studied in acetonitrile solution, which included static adsorption, dynamic adsorption and selectivity experiments. Typically, static adsorption experiments were carried out by dispersing 20 mg polymer microspheres into 2.0 mL acetonitrile solutions containing different concentrations of 17β-E2 (1, 10, 20, 40, 60, 80 and 100 mg/L) in 10 mL colorimetric tubes. After being shaken for 24 h at room temperature, the samples were isolated using an external magnet. The residual concentration of 17β-E2 in the supernatant solution was determined by HPLC-UV. The adsorbed amount of 17β-E2 was calculated by subtracting the residual amount from its total amount. Dynamic adsorption experiments were performed with 20 mg polymer microspheres dispersed into 2.0 mL acetonitrile solutions containing 60 mg/L 17β-E2. After stirring for 10, 30, 60, 90, 120, 180 and 270 min, respectively, the solution was separated and quantified by HPLC-UV. Selectivity experiments were conducted by comparing the binding capacities of the polymer microspheres between 17β-E2 and its structural analogues (E3, 17α-E2, E1, BPA, DES, HS and DS). Briefly, 20 mg polymer microspheres were dispersed into 2.0 mL acetonitrile solutions containing 60 mg/L different kinds of PEEs, and after being shaken for 24 h at room temperature, the supernatant was quantified by HPLC-UV. All tests were determined in triplicate.

2.6. MMIMs applied in magnetic solid phase extraction for analysis of real samples

Seawater samples were randomly collected from the surface seawater of Yellow Sea, lake water samples were collected from Sanyuan Lake, and soil samples were obtained from a suburb, which were all located in coastal zone of Yantai City. Yogurt samples were purchased from a local market of Laishan District. These samples were simply extracted as follows. For the seawater, lake water and yogurt samples, 1 mL samples were added into 10 mL acetonitrile solution, and after being shaken for 30 min, the solutions were centrifuged and filtered, and the extract solutions were obtained. For the solid samples, 2.0 g soil samples were dispersed into 20 mL acetonitrile solution and then shaken for 1 h. The supernatants were centrifuged and filtered with 0.45 μm microfiltration membrane. All the sample extract solutions were stored at 4 °C for use.

The process of magnetic solid phase extraction (MSPE) was carried out according to that reported[21–23] with suitable modification. Specifically, MMIMs of 80 mg were dispersed into 2 mL sample extract solutions spiked with 17β-E2 at three concentrations (0.1, 1.0 and 10 mg/L). After being shaken for 3 h at room temperature, the MMIMs sorbent loaded with 17β-E2 was separated from the suspension using a magnet and the supernatant was measured by HPLC-UV. Subsequently, the 17β-E2 adsorbed onto the MMIMs sorbent was eluted with 2 mL of methanol-acetic acid solution (9:1, v/v). Then the eluent was dried and re-dissolved in 2 mL acetonitrile and then determined by HPLC-UV. Finally, after the extraction process, in order to reuse the same sorbent for new extraction of the 17β-E2, the MMIMs were washed with methanol-acetic acid solution and acetonitrile for several times. Then the sorbent was dried at 60 °C for new extraction. The MSPE procedure was illustrated in Fig. 1.

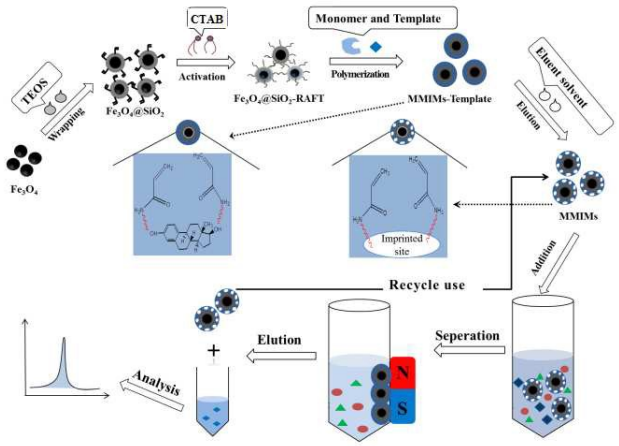

Fig. 1 Schematic illustration of the preparation process of MMIMs by RAFT precipitation polymerization, and MSPE application for recognition and removal of 17β-E2.

3. Results and discussion

3.1. Preparation and characterization of the MMIMs

Fig. 1 displays the preparation process of MMIMs by one-pot RAFT precipitation polymerization, and the MSPE procedure for MMIMs application. The core-shell MMIMs were prepared in a mild condition with one-pot approach, which allowed all reagents to be added and to react together. The RAFT polymerization procedure was simple to avoid complex surface modification, and one-pot setting simplified experimental process and shortened synthetic period. And then, the obtained MMIMs were fully characterized by TEM, FT-IR, TGA, VSM and BET as follows.

Fig. 2 shows the morphologies of products at different synthetic stages. $Fe_3O_4@SiO_2$ (Fig. 2A) and MMIMs (Fig. 2B) particles were monodisperse and exhibited regular sphere morphology, which indicated the polymerization smoothly proceeded on the surface of $Fe_3O_4@SiO_2$ by RAFT. By comparing Fig. 2A and B, the thickness of the imprinting shell layer could be attained within 10–30 nm (Fig. 2B). Owing to the thin imprinting layers, almost all the template molecules could be completely eluted and thereby produce the largest amounts of imprinted cavity sites, resulting in high binding capacities and fast mass transfer. However, the MMIMs-Control and MNIMs particles were not uniform in size and distribution, with the average diameter ranging from 225 to 505 nm (Fig. 2C) and from 730 to 1500 nm (Fig. 2D), respectively, which was adverse to mass transfer. When $Fe_3O_4@SiO_2$ without further RAFT functionalization was used, imprinting layers could not form around the magnetic particles, but non-magnetic secondary

particles form by precipitation polymerization with much smaller diameters (100–200 nm), as shown in Fig. 2C. The secondary particles might well adhere with the magnetic particles, and thereby cause inhomogeneous size and distribution of the MMIMs-Control (Fig. 2C). For MNIMs, as seen in Fig. 2D, their sizes were quite large with a wide distribution, which was quite different from MMIMs. This was very likely owing to the absence of template in the RAFT polymerization. For the MNIMs, without the presence of template molecules, the crosslinking substances all containing double bonds could more easily form shell-layers on the surface of Fe_3O_4@SiO_2, and thereby result in thicker shell-layers and easier aggregation, presenting non-homogeneous and much larger material (Fig. 2D).

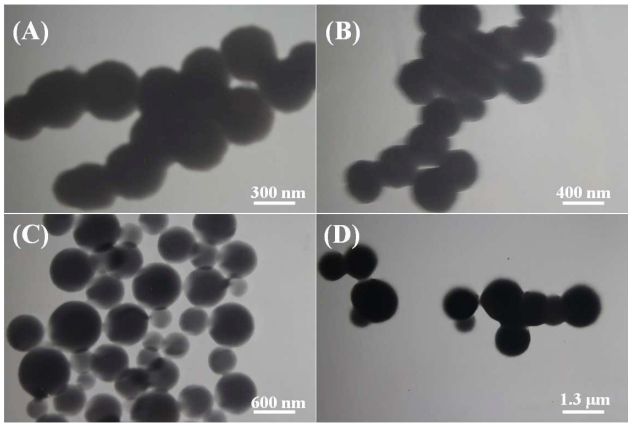

Fig. 2 TEM images of Fe_3O_4@SiO_2 (A), MMIMs (B), MMIMs-Control (C) and MNIMs (D) particles.

Fig. 3A shows the FT-IR spectra of Fe_3O_4, Fe_3O_4@SiO_2, Fe_3O_4@SiO_2-RAFT, MMIMs and MNIMs particles. The polymerization process could be evaluated according to the characteristic functional groups. The characteristic absorption band of Fe_3O_4 was at 580 cm^{-1} (curve a). The absorption at 803 and 1089 cm^{-1} could be attributed to the stretching vibration of Si-O and Si-O-Si, respectively, proving that SiO_2 was successfully covered on Fe_3O_4 particles (curve b). As seen from curve c, the peak at 1629 cm^{-1} represented the stretching vibration of C=C bond of alkene, due to the RAFT active modification on the surface of Fe_3O_4@SiO_2. The unique absorption peak at 1728 cm^{-1} belonged to the stretching vibration of C=O bond, the typical peak at 2998 and 2955 cm^{-1} could be ascribed to the saturated C-H bond, as well as the peaks at 1392 and 1260 cm^{-1} could be assigned to the C-N bond, indicating the imprinted polymer layer was grafted onto the surface of Fe_3O_4@SiO_2 successfully, as demonstrated in curve d. In addition, the peak at 1462 cm^{-1} belonged to the aromatic carbon-carbon bond of DVB which was used for the preparation of the polymer. The FT-IR spectrum of MNIMs (curve e) looks exactly the same as that of MMIMs (curve d), except for the lower intensity. All the results of FT-IR confirmed that the core-shell structured MMIMs were successfully prepared by RAFT precipitation polymerization.

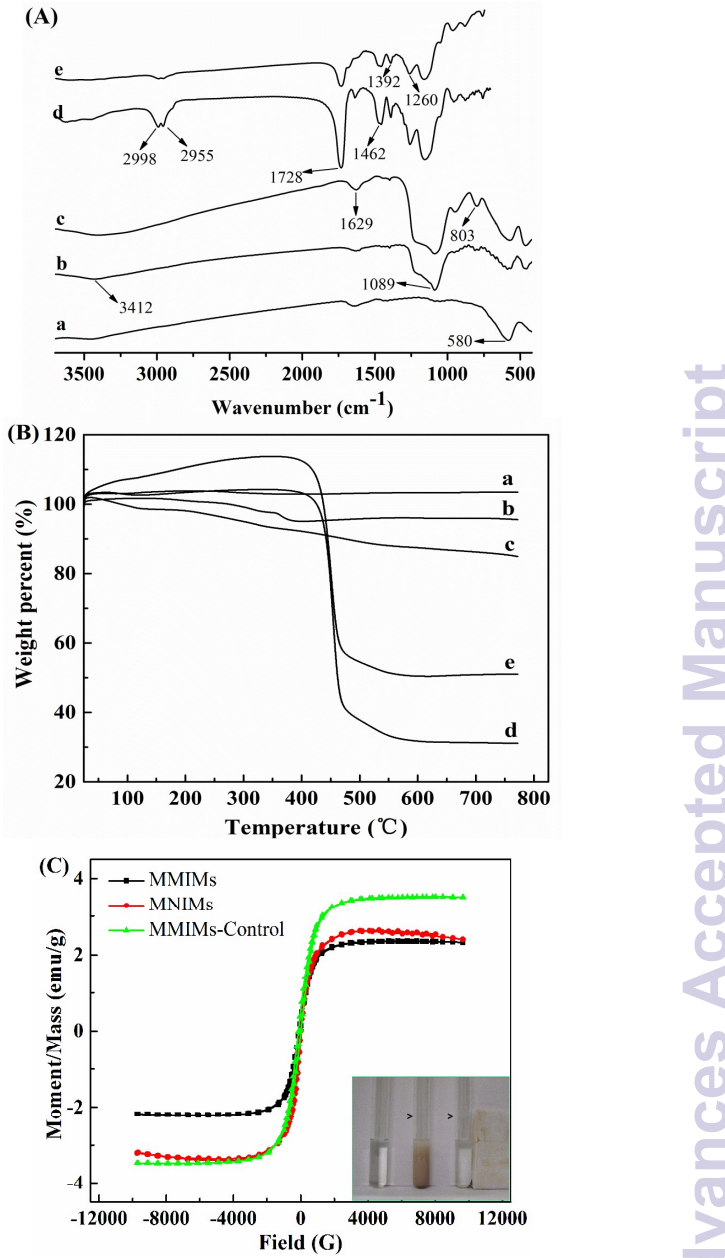

Fig. 3 (A) FT-IR spectra and (B) TGA curves of Fe_3O_4 (a), Fe_3O_4@SiO_2 (b), Fe_3O_4@SiO_2-RAFT (c), MMIMs (d) and MNIMs (e). (C) Magnetic hysteresis loops of MMIMs, MNIMs and MMIMs-Control, and the insert shows the dispersion and separation process of a 17β-E2 solution in absence (left) and presence (middle) of MMIMs and in the presence of an external magnetic field (right).

The corresponding TGA results of the above five particles were displayed in Fig. 3B. As seen, the TGA curve of Fe_3O_4 was almost a straight line, indicating the particles was very pure without impurities (curve a). There was a slight weight loss at 250–350°C for Fe_3O_4@SiO_2 particles (curve b), which could be attributed to the dehydration of the SiO_2 layer. As observed from curve c, Fe_3O_4@SiO_2-RAFT exhibited bigger weight loss, which may be due to the pyrolysis of RAFT active groups. The TGA curves of MMIMs (curve d) and MNIMs (curve e) particles dropped rapidly at around 450 °C, suggesting that the whole imprinted and non-imprinted polymer layers on the surface of Fe_3O_4@SiO_2 largely decomposed under high temperature,

Cite this: DOI: 10.1039/c0xx00000x

www.rsc.org/xxxxxx

ARTICLE TYPE

respectively. In addition, the peak temperatures of MMIMs and MNIMs were 454.36 and 451.72 °C, respectively, and the corresponding residual amounts were 25.61 and 36.30%, respectively, as could be obtained from the TGA results in Table S1 and DTG curves in Fig. S1. The results demonstrated that the MMIMs possessed higher polymerization efficiency and good thermal stability below 400 °C.

Fig. 3C shows the magnetic hysteresis loops analysis of the MMIMs, MMIM-Control and MNIMs, and the inset illustrates the dispersion and agglomeration processes of the MMIMs. It is seen that there is a similar general shape to the three curves, although the saturation magnetization value of MMIMs is low (Table S2). The results suggested that the prepared MMIMs were magnetically responsive. As seen from Table S2, the MMIMs had better magnetic induction intensity, and this may be caused by the strong magnetism of independent Fe_3O_4@SiO_2 particles which did not participate in the reaction. Consequently, the homogeneously dispersed MMIMs could go straight towards the magnet and adhere to the inner side wall of the vials when the external magnetic field was applied, and the turbid solution became clear and transparent, as evidenced in the inset of Fig. 3C, showing a fast and simple magnetic separation.

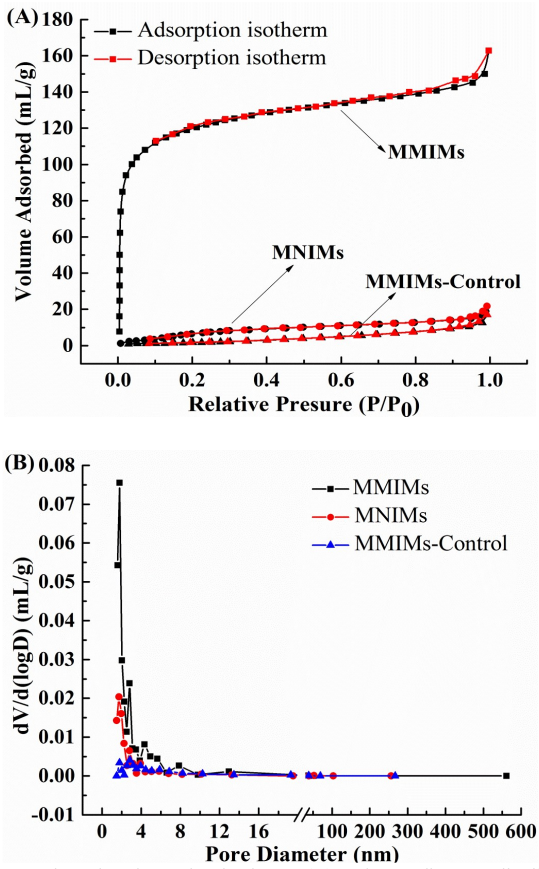

Fig. 4 N_2 adsorption-desorption isotherms (A) and pore diameter distribution curves (B) of MMIMs, MNIMs and MMIMs-Control.

The N_2 adsorption-desorption isotherms and pore diameter distribution of MMIMs, MMIMs-Control and MNIMs were shown in Fig. 4. The type IV isotherm curves with a loop were observed for MMIMs (Fig. 4A), which indicated that MMIMs had a well-defined porous structure. As seen, the MMIMs showed a hysteresis loop, where the desorption curve was closer but slightly leveled above the adsorption curve, representing that the MMIMs were stable with low swelling and low solvent uptake.[24] The narrow pore size distribution and low average pore diameter displayed from the adsorption plot (Fig. 4B) suggested that the size of the cavities formed in the MMIMs matrix played an important role in binding capacity. The structure parameters of the three microspheres obtained by BET analysis were listed in Table S3. As seen, the specific surface area, cumulative pore volume and average pore diameter of MMIMs particles were 444.86 m^2/g, 0.10 mL/g and 4.18 nm, respectively, while MMIMs-Control particles were 6.89 m^2/g, 0.030 mL/g and 7.96 nm, and MNIMs particles were 46.18 m^2/g, 0.038 mL/g and 4.35 nm, respectively. Obviously, the specific surface area and cumulative pore volume of MMIMs were much larger while the average pore diameter was slightly smaller than that of the latter two. The large specific surface area proved that MMIMs had uniform, regular spherical structure (Fig. 2B). Generally, MIPs have slight differences in surface area and pore volume from NIPs. Here, the significantly high values of MMIMs might well be attributed to the template functioning somehow with the RAFT polymerization. During MMIMs preparation, when the template molecules were added, the synthesis would become a doping synthesis to some extent. This would produce thinner imprinting shell-layers with smaller diameters, along with amounts of imprinted cavities, and therefore would lead to large surface area and pore volume.

3.2. Binding properties of the MMIMs

The binding ability of MMIMs was investigated by performing the static, dynamic and selectivity studies. Fig. 5A shows the static binding isotherms of 17β-E2 onto three polymers. As seen, the adsorption capacity for 17β-E2 increased quickly as its initial concentration increasing. When the equilibrium concentration was higher than 60 mg/L, adsorption amounts of MMIMs became stable and its recognition sites were almost occupied by 17β-E2. MMIMs-Control and MNIMs displayed the same trends, but lower saturated adsorption amounts. Hence, the MMIMs exhibited significantly high 17β-E2 loading. Moreover, according to the Scatchard equation,[25] the K_d (equilibrium dissociation constant) and Q_{max} (maximum adsorption capacity) were calculated, *i.e.*, 30.6 μmol/L and 2.92 μmol/g for MMIMs, and 47.5 μmol/L and 0.76 μmol/g for MNIMs, respectively, and thereby the imprinting factor was attained of 3.84. The results suggested that the MMIMs had specific binding sites for template molecule.

To evaluate the binding isotherms of MMIMs, four adsorption isotherm models including Langmuir, Freundlich, Redlich-Peterson and Langmuir-Freundlich were employed,[24] as shown in Fig. 5B. Their corresponding equations and parameters for adsorption of 17β-E2 onto the three polymers were listed in Table S4. Detailed descriptions for model fitting were given in electric supplementary information (ESI). It can be seen that for all the three polymers, the Langmuir-Freundlich isotherm model yielded the best fitting among the four models, for correlation coefficients (R^2) of 0.9995, representing its ability to simultaneously model both subsaturation and saturation behaviors.[26] In addition, the MMIMs provided the highest concentration of binding sites per gram of polymers (Nt= 212.8 μmol/g) and the largest median binding affinity (α= 5.677 g/μmol), indicating an excellent imprinting effect due to the presence of a number of specific binding sites on the MMIMs.

Dynamic binding experiments were conducted to assess the mass transfer properties of the MMIMs. Fig. 6A shows the time-dependent increase in the amount of 17β-E2 adsorbed by MMIMs and MMIMs-Control. As can be seen, the MMIMs demonstrated significantly higher dynamic binding performances than that of MNIMs, which indicated the uniform spherical structure and larger specific surface area of the MMIMs were favorable to rapid mass transfer.

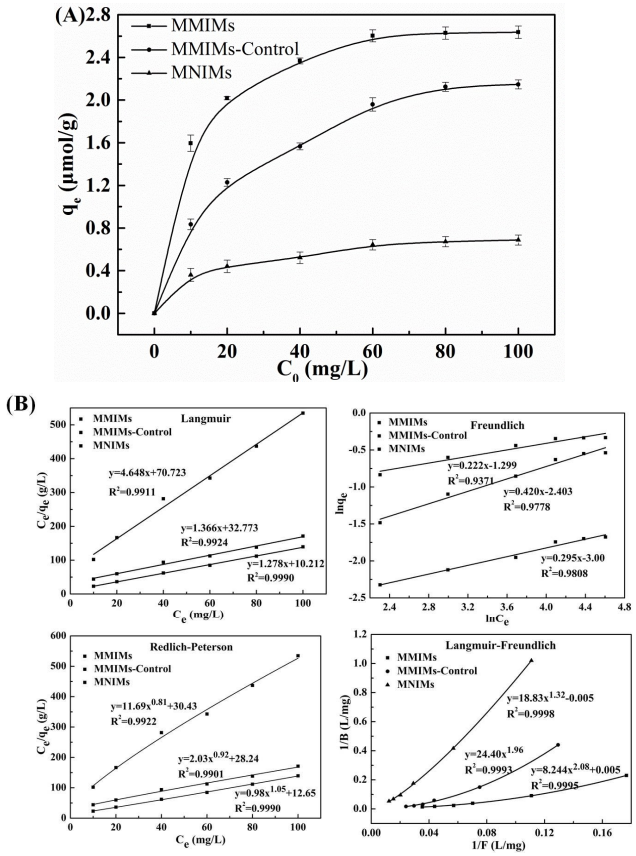

Fig. 5 (A) Static adsorption isotherms of 17β-E2 onto MMIMs, MMIMs-Control and MNIMs and (B) Langmuir, Freundlich, Redlich-Peterson and Langmuir-Freundlich isotherm models for 17β-E2 adsorption process. Experimental conditions: V, 2 mL; polymer, 20 mg; adsorption time, 12 h; room temperature.

As for the dynamic models of MMIMs, pseudo-first-order, pseudo-second-order, Elovich and intraparticle diffusion[27–29] for 17β-E2 were displayed in Fig. 6B, and the related equations and fitting results were listed in Table S5. Detailed descriptions for the model fitting could be found in ESI. As seen, the pseudo-second-order model could better describe the time effect on the adsorption system than other kinetic models, which provided the most suitable correlation for the adsorption, with the highest correlation coefficient of 0.9966. The pseudo-second-order equation can be expressed as:

$$\frac{t}{q_t} = \frac{1}{k_2 q_e^2} + \frac{t}{q_e} \qquad (1)$$

where, q_t is the instantaneous adsorption amount of 17β-E2 in the adsorbent at time t, k_2 is the adsorption rate constant, and q_e is the adsorption amount at equilibrium. The obtained q_e of 2.81 μmol/g calculated from the pseudo-second-order model agreed well with the q_e of 2.64 μmol/g from experimental results. So, the adsorption could be deduced to follow the pseudo-second-order kinetics model.

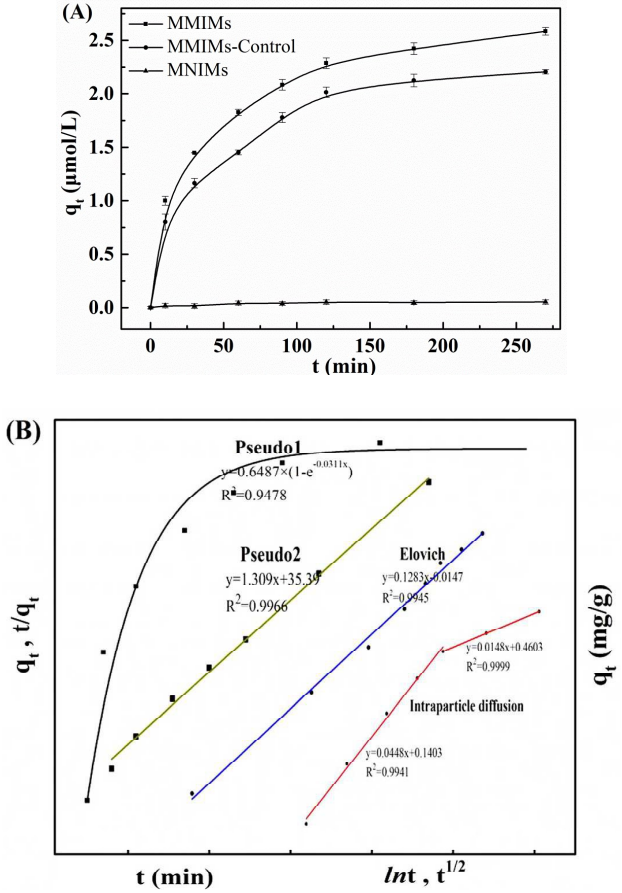

Fig. 6 (A) Kinetic binding of 17β-E2 onto MMIMs, MMIMs-Control and MNIMs and (B) Pseudo-first-order, Pseudo-second-order, Elovich and intraparticle diffusion kinetic models for 17β-E2 towards MMIMs. Experimental conditions: template concentration, 60 mg/L; V, 2 mL; polymer, 20 mg; room temperature.

In order to evaluate the competitive recognition ability of the obtained MMIMs, seven PEEs (E3, 17α-E2, DS, BPA, DES, HS

Cite this: DOI: 10.1039/c0xx00000x

www.rsc.org/xxxxxx

ARTICLE TYPE

and E1) as structural analogues were used. As seen from Fig. 7A (up), MMIMs presented a higher binding capacity for 17β-E2 than that for those competitive PEEs. The binding capacities and selectivity factors of the MMIMs for E3, 17α-E2 and DS were close and higher than the other four PEEs, as their structures are more similar to that of 17β-E2 (Fig. 7A, below). Meanwhile, compared with MMIMs-Control, the MMIMs showed obviously higher binding capacity, revealing the utilization of RAFT as an idea strategy could greatly improve binding capacity and mass transfer rate of imprinted materials. However, MNIMs adsorbed much less template molecules, and there was no significant difference in binding capacity between the competitive PEEs and 17β-E2, since there was no tailor-made recognition sites formed in the MNIMs. Therefore, the obtained MMIMs could selectively recognize the delicate difference of 17β-E2 from its analogues.

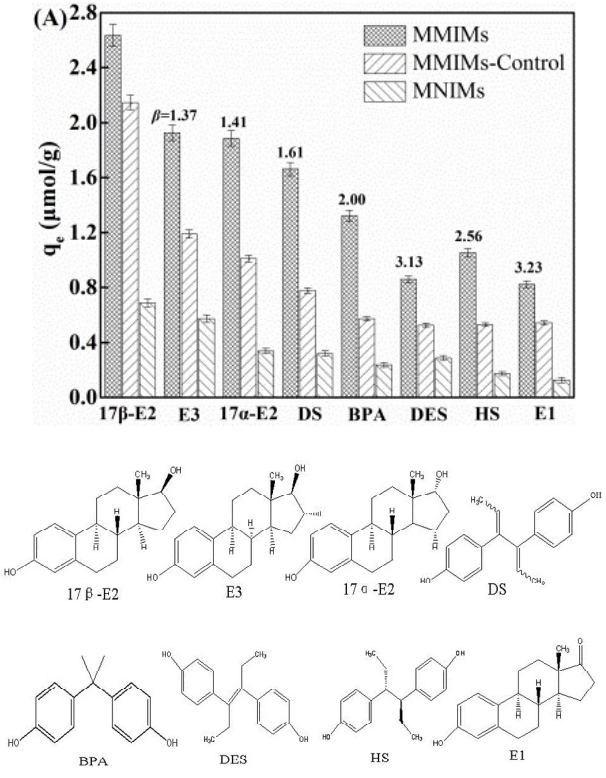

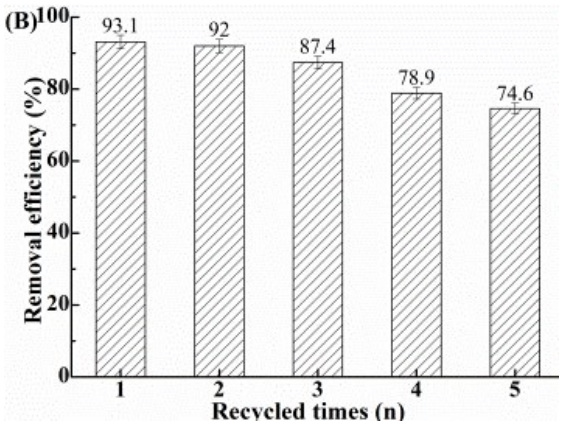

Fig. 7 (A) Binding capacities of MMIMs, MNIMs and MMIM-Control for eight PEEs (up), and their chemical structures (below). (B) Removal efficiency of MMIMs-MSPE in five recycled times. (Experimental conditions for (A): polymer, 20 mg; 17β-E2 concentration, 60 mg/L; V, 2.0 mL; adsorption time, 24 h; room temperature. The selectivity factor was marked β = q(template)/q(competitive molecule); and (B) polymer, 80 mg; 17β-E2, 1.0 mg/L; V, 2.0 mL; incubating time, 3 h; eluting, 2 mL methanol-acetic acid solution (9:1, v/v); redissolved solution, 2.0 mL acetonitrile.)

3.3. Application of MMIMs to removal of 17β-E2

The MMIMs were used as the sorbents in SPE process, *i.e.*, magnetic SPE was performed. To test the stability and reusability of the MMIMs-MSPE, five binding/removal cycles were conducted. Fig. 7B displays the removal efficiency of MMIMs for 1 mg/L 17β-E2 after 5 recycles. As observed, the removing efficiencies were attained of 93.1, 92.0, 87.4, 78.9 and 74.6%, respectively. It showed the magnetic separation under an external magnetic field could easily and rapidly be accomplished, and the MMIMs could effectively remove 17β-E2 at least five recycles.

Table 1. MMIMs-MSPE recoveries (%) and relative standard deviations (RSD, %) obtained from analysis of four different samples spiked with 17β-E2.[a)]

Samples	Spiked concentration (mg/L)		
	0.1	1.0	10.0
Seawater	76.7[b)]±4.9[c)]	82.7±2.7	74.2±3.4
Lake water	86.4±4.7	75.6±4.4	71.7±2.8
Soil	108.3±4.7	93.4±2.6	105.8±3.0
Yogurt	88.9±1.5	96.0±1.1	100.3±6.0

[a)] Experimental conditions: polymer, 80 mg; sample volume, 2 mL; incubating time, 3 h; separation, magnet; eluting, 2 mL methanol-acetic acid solution (9:1, v/v); redissolved solution, 2 mL acetonitrile.

[b)] Average value from three individual experiments.

[c)] $n = 3$.

In order to assess the practical applicability of MMIMs-MSPE, several real samples of water, soil and food were analyzed. Table 1 lists the removal recoveries of MMIMs applied in

seawater, lake water, soil and yogurt samples spiked at three concentration levels of 17β-E2. Satisfactory recoveries were obtained, such as 76.7–108.3 with precision of 1.5–4.9% at 0.10 mg/L. The MMIMs were demonstrated potentially applicable for highly efficient preconcentration and separation of 17β-E2 in real samples. Fig. S2 presents the typical HPLC-UV chromatograms. As seen, the matrix effects were reduced and the spiked 17β-E2 compounds were concentrated by the MMIMs-MSPE, indicating that the MMIMs had excellent imprinting efficiency. Meanwhile, the magnetic property would enable the MMIMs-MSPE more attractive. Compared to conventional SPE, a simpler and faster magnetic separation and enrichment procedure was provided dispensing with pretreatments such as filtration and centrifugation.

4. Conclusions

In summary, a convenient and cost-effective magnetic core-shell imprinted microsphere for selective recognition and effective removal of 17β-E2 in complicated matrices was prepared through one-pot synthesis by RAFT living precipitation polymerization. The obtained MMIMs showed strong response to an external magnetic field with a rapid removal efficiency and displayed high binding capacity and selectivity towards the template. The MMIMs offered satisfactory recoveries for template when used for MSPE and were successfully applied in the enrichment and removal of trace 17β-E2 from environmental and food samples with good stability and repeatability. This work provided an excellent platform for the removal of PEEs and demonstrated a bright future for matrices purification and pollution abatement.

Acknowledgements

This work was financially supported by the National Natural Science Foundation of China (21105117, 31160317, 21175084, 21307052 and 21275068), the Natural Science Foundation of Shandong Province of China (ZR2013BL006), and the Key Laboratory of Coastal Zone Environmental Processes, YICCAS (201207).

[a] *Key Laboratory of Coastal Environmental Processes and Ecological Remediation, Shandong Provincial Key Laboratory of Coastal Environmental Processes, Yantai Institute of Coastal Zone Research, Chinese Academy of Sciences, Yantai 264003, China. Tel/Fax: +86 535 2109130, E-mail address: lxchen@yic.ac.cn (L. Chen).*

[b] *State Key Laboratory of Food Science and Technology, Nanchang University, Nanchang 330047, China. Tel/Fax: +86 791 6634810, E-mail address: huaxiong100@126.com (H. Xiong).*

[c] *Key Lab in Molecular and Nanomaterials Probes of the Ministry of Education of China, College of Chemistry, Chemical Engineering and Materials Science, Shandong Normal University, Jinan 250014, China. Tel.: +86 531 86180740; Fax: +86 531 82615258. E-mail address: dzshen@sdnu.edu.cn (D. Shen).*

[d] *School of Chemistry & Chemical Engineering, Linyi University, Linyi 276005, China.*

***** *Corresponding authors.*

[1] *Equally contributed to this work.*

†Electric supplementary information (ESI) available. See DOI: 10.1039/b000000x

Notes and references

1 J. Kaiser, *Science*, 2000, **290**, 695.
2 N. Yildirim, F. Long, C. Gao, M. He, H. Shi and A. Gu, *Environ. Sci. Technol.*, 2012, **46**, 3288.
3 P. Matthiessen and I. Johnson, *Environ. Pollut*., 2007, **146**, 9.
4 M. Maynadier, P. Nirdé, J. Ramirez, A. Cathiard, N. Platet, M. Chambon and M. Garcia, *Hormonal Carcinogenesis V, Springer New Yor*k, 2008, 485.
5 Z. Meng, W. Chen and A. Mulchandani, *Environ. Sci. Technol*., 2005, **39**, 8958.
6 L. Chen, S. Xu and J. Li, *Chem. Soc. Rev.*, 2011, **40**, 2922.
7 J. Ma, L. Yuan, M. Ding, S. Wang, F. Ren, J. Zhang and X. Zhou, *Biosens. Bioelectron*., 2011, **26**, 2791.
8 Y. Shi, D. Peng, C. Shi, X. Zhang, Y. Xie and B. Lu, *Food Chem.*, 2011, **126**,1916.
9 M. Noir, F. Plieva, T. Hey, B. Guieysse and B. Mattiasson, *J. Chromatogr. A*, 2007, **1154**, 158.
10 G. Pan, Y. Zhang, X. Guo, C. Li and H. Zhang, *Biosens. Bioelectron*., 2010, **26**, 976.
11 M. Titirici and B. Sellergren, *Chem. Mater*., 2006, **18**, 1773.
12 S. Xu, J. Li and L. Chen, *Talanta*, 2011, **85**, 282.
13 S. Xu, J. Li and L. Chen, *J. Mater. Chem*., 2011, **21**, 4346.
14 T. Zhou, L. Jorgensen, M. Mattebjerg, I. Chronakis and L. Ye, *RSC Adv.*, 2014, **4**, 30292.
15 S. Xu, C. Guo, Y. Li, Z. Yu, C. Wei and Y. Tang, *J. Hazard. Mater.*, 2014, **264**, 34.
16 C. Alvarez lorenzo, C. Gonzalez Chomon and A. Concheiro, *Smart Materials for Drug Delivery*, 2013, **2**, 228.
17 G. Martins, J. Mano and N. Alves, *Langmuir*, 2011, **27**, 8415.
18 Y. Li, X. Li, J. Chu, C. Dong, J. Qi and Y. Yuan, *Environ. Pollut*., 2010, **158**, 2317.
19 S. Xu, J. Li, X. Song, J. Liu, H. Lu and L. Chen, *Anal. Methods*, 2013, **5**, 124.
20 Y. Li, C. Dong, J. Chu, J. Qi and X. Li, *Nanoscale*, 2011, **3**, 280.
21 P. Dramou, P. Zuo, H. He, L. Pham-Huy, W. Zou, D. Xiao and C. Pham-Huy, *J. Chromatogr. A*, 2013, **1317**, 110.
22 T. Jiang, L. Zhao, B. Chu, Q. Feng, W. Yan and J. Lin, *Talanta*, 2009, **78**, 442.
23 P. Manesiotis, L. Fitzhenry, G. Theodoridis and P. Jandera, *Anal. Tech. Scientists*, 2012, **4**, 457.
24 R. Krupadam, B. Bhagat, S. Wate, G. Bodhe, B. Sellergren and Y. Anjaneyulu, *Environ. Sci. Technol*., 2009, **43**, 2871.
25 E. Zoelen, R. Kramer, H. Moerkerk and J. Veerkamp, *Trends Pharmacol. Sci*., 1998, **19**, 487.
26 W. Ma, F. Ya, M. Han and R. Wang, *J. Hazard. Mater*., 2007, **143**, 296.
27 Y. Ho and G. McKay, *Process Biochem*., 1999, **34** , 451.
28 J. Zhu, S. Wei, H. Gu, S. Rapole, Q. Wang, Z. Luo and Z. Guo, *Environ. Sci. Technol*., 2011, **46**, 977.
29 X. Cai, J. Li, Z. Zhang, F. Yang, R. Dong and L. Chen, *ACS Appl. Mater. Interfaces*, 2014, **6**, 305.